

Nanoscale Abrasive Wear of Polyethylene: A Novel Approach To Probe Nanoplastics Release at the Single Asperity Level

Ehsanur Rahman,^{II} Sara BinAhmed,^{II} Phoebe Keyes, Claire Alberg, Stacy Godfrey-Igwe, Greg Haugstad, and Boya Xiong^{*}



Cite This: *Environ. Sci. Technol.* 2024, 58, 13845–13855



Read Online

ACCESS |

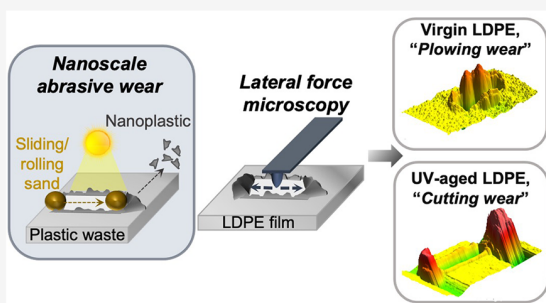
Metrics & More

Article Recommendations

Supporting Information

ABSTRACT: There is a growing concern that nanoplastic pollution may pose planetary threats to human and ecosystem health. However, a quantitative and mechanistic understanding of nanoplastic release via nanoscale mechanical degradation of bulk plastics and its interplay with photowear remains elusive. We developed a lateral force microscope (LFM)-based nanoscratch method to investigate mechanisms of nanoscale abrasive wear of low-density polyethylene (LDPE) surfaces by a single sand particle (simulated by a 300 nm tip) under environmentally relevant load, sliding motion, and sand size. For virgin LDPE, we found plowing as the dominant wear mechanism (i.e., deformed material pushed around the perimeter of scratch). After UVA-weathering, the wear mechanism of LDPE distinctively shifted to cutting wear (i.e., deformed material detached and pushed to the end of scratch). The shift in the mechanism was quantitatively described by a new parameter, which can be incorporated into calculating the NP release rate. We determined a 10-fold higher wear rate due to UV weathering. We also observed an unexpected resistance to initiate wear for UV-aged LDPE, likely due to nanohardness increase induced by UV. For the first time, we report $0.4\text{--}4 \times 10^{-3} \mu\text{m}^3/\mu\text{m}$ sliding distance/ μN applied load as an initial approximate nanoplastic release rate for LDPE. Our novel findings reveal nanoplastic release mechanisms in the environment, enabling physics-based prediction of the global environmental inventory of nanoplastics.

KEYWORDS: nanoplastics, mechanical degradation of polymer, lateral force microscopy, nanoscale wear, photooxidation, fragmentation, nanotribology



INTRODUCTION

Plastic breakdown products, micro- and nanoplastics (MPs and NPs),^{1,2} pose urgent threats to human health,^{3–5} ecosystem functions,^{6–9} and global climate.^{10–12} NPs (size $<1 \mu\text{m}$) are potentially more harmful than MPs because of their higher extent of environmental transport and exposure to organisms and size-dependent toxicity effects.^{13–15} NPs are generated from photodegradation,^{16,17} mechanical fragmentation/abrasion,^{18–21} and thermal degradation^{21–23} of bulk plastics. Specifically, mechanical degradation is recognized as a critical mechanism in many scenarios^{20,24–26}; however, it remains poorly quantitatively and mechanistically understood. Unlike photodegradation in which UV-dose translates data from the laboratory to the field,²⁷ current mechanical degradation methods (e.g., the rotational speed of a shaker^{28,29}) cannot quantify the input energy or force.¹⁶ A few studies attempted to quantify the input energy deployed mN-kN range load, generating primarily MPs.^{18,26,30} Mechanical processes that specifically release NPs remain unexplored.

In addition to sequential *bulk* fragmentation of photodegraded plastics,^{31–33} a growing literature has highlighted the role of *surface* degradation for MP/NP release.^{16,34} Surface mechanical degradation of plastics can be described as various

modes of wear (adhesive, abrasive, and fatigue^{35,36}), resulting from the relative motion between two contacting surfaces. In particular, abrasive wear³⁷ is the deformation of *soft* material caused by collision or sliding of *hard* solid and/or protruding features (e.g., roughness³⁸). Frequently, soft plastics co-occur with hard inorganic particles (their hardness differs by 1–2 decades^{39,40}), during their co-transport in wind and soil erosion,⁴¹ storm runoff,²⁴ and beaches.²⁸ Thus, compared to other wear mechanisms, we hypothesize that abrasive wear is one of the dominant mechanisms that directly generates NPs in the environment.

Previous abrasive wear studies are mostly at the micro- and macroscale, utilizing abrasive papers,^{26,30} pin-on-disk devices,^{42,43} and abrasive slurry,⁴⁴ generating micrometer-scale wear debris. Limited studies have investigated the mechanisms and rates of *nanoscale* abrasive wear that predominantly

Received: November 18, 2023

Revised: May 26, 2024

Accepted: May 29, 2024

Published: June 14, 2024



releases NPs. Atomic force microscopy (AFM), in particular, lateral force microscopy (LFM), is ideal for mechanistically exploring nanoscale abrasive wear,^{45,46} as the AFM tip can simulate a single asperity contact with a solid surface. LFM utilizes a scan perpendicular to the cantilever axis, resulting in friction-actuated cantilever torsion, which can be captured as a lateral deflection to yield absolute friction force.⁴⁷ Thus, LFM offers nanoscale spatial resolution of friction and topography under a controlled normal load. This approach has enabled the mapping of nanoscale wear of inorganic^{48–50} or carbonaceous materials⁵¹ but has not been widely utilized for detailed wear mechanism and rates analysis for polymers, particularly polyolefins.⁵² Furthermore, such an approach has not been used for studying photooxidized polymers. For semicrystalline polyolefins, photooxidation is known to cause substantial MW reduction, oxidation, chemicrystallization, and loss of bulk ductility.⁵³ Very limited studies examined the effect of UV⁵⁴ or gamma irradiation⁵⁵ on microscale wear. However, the effect of photooxidation on surface nanomechanical properties and nanoscale abrasive wear behavior remains unknown.

Here, we developed a novel LFM-based nanoscratch test, followed by imaging, to explore the fundamental mechanisms and rates of nanoscale abrasive wear of low-density polyethylene (LDPE) and the impact of photowear. Through nanoscale control and measurement of forces and topography, our method enables us to (1) apply forces that are relevant in natural sediment transport, (2) elucidate the onset and mechanisms of nanoscale abrasive wear at the single-asperity level, and (3) quantify wear rate per unit force as an approximate nanoplastic release by sand abrasion via sliding motion. To the best of our knowledge, this is the first time such a method has been applied to polymer materials to inform nanoplastic release mechanisms in the environment and to demonstrate the contrasting wear behavior of LDPE at the nanoscale before and after UV-weathering.

MATERIALS AND METHODS

Material and Photooxidation of LDPE. A commercial LDPE homopolymer film (101.6 μm thick, BFI345-013, Blueridge Films Inc., VA, USA) was studied as a model polyolefin. After DI water rinsing and overnight drying, the LDPE films were weathered using a QUV/SE (Q-Lab, Ohio, USA) at 1.55 W/m² (340 nm) and 60 °C for 50 days without condensation (ASTM G154). No temperature or humidity was changed during the UV aging of LDPE. Facile breakage of the film when transferred by tweezers suggested that the UV exposure resulted in complete LDPE embrittlement. A ~1 × 1.5 cm LDPE piece was glued to a glass slide using epoxy for all AFM experiments.

Friction Measurements. LFM was used to explore the sliding friction characteristics between the LDPE samples and silica under dry conditions by using an MFP3D-Bio Atomic Force Microscope (Asylum Research, Santa Barbara, CA). A rounded silicon probe (SD-R150-FM-10, NanoAndMore USA Corp., Santa Clara, CA) with a radius of 150 nm and a spring constant of 3.5 N/m was used. The size and chemistry of the probe were selected to represent fine sediments or sand surface nanoroughness.^{38,56,57} Although natural sand and soil grains range from 0.1 to 10 mm in diameter, their surface roughness at both vertical and lateral scales has been determined to be sub-μm to a few μm using optical interferometry.^{38,56,58,59} Such a range of roughness has also been deployed for studying roughness effects on porous media asperities⁵⁷ and pore-scale³⁸

transport. The normal spring constants of all probes used in this study were calibrated using the thermal noise method⁶⁰ in conjunction with collecting force-Z curves on freshly cleaved mica to determine the optical lever sensitivity.

To measure friction and loading force, lateral deflection and the z-sensor were simultaneously collected at constant vertical cantilever deflection (i.e., measured normal load). Friction force was quantified as the difference of the lateral signals of trace (sliding in one direction) and retrace (sliding in the opposite direction) with a sign included (i.e., friction loop)⁴⁷ using Gwyddion (version 2.59). For friction force maps (*x* and *y* scan enabled), the wearless frictional regime was probed under 50 nN, 128 points/loop, and 128 loops in total at a rate of 0.25 Hz. For friction measurements as a function of load, a built-in software function was used to automate load ramping at each friction loop for 64 loops from zero until the maximum set load was reached. The raw lateral signals in V to absolute friction force in nN was converted using eq 1 with the LFM measurements using the same silica probe on mica and the known coefficient of friction between mica and silicon (0.168⁶⁰):

$$f = \frac{(\text{lateral trace signal} - \text{lateral retrace signal})}{2} \times \frac{\mu_{\text{mica}}}{m} \quad (1)$$

where *f* is the friction, *m* is the slope of raw lateral signals in V versus normal load on a clean mica, and μ_{mica} is the coefficient of friction of silicon on mica (Figure S1 and Table S1). Proper tip cleaning and quality control were performed to ensure the consistency of tip status between different friction experiments (Figure S2). Both friction experiments were repeated on 5 different spots on the same coupon for each sample.

Nanoscratch Abrasion Experiments. A nanoscratch test was developed to perform the single asperity abrasive wear of LDPE at the nanoscale, followed by topography imaging (details in the SI). A rounded silicon tip (SD-R150-NCL-10, NanoAndMore, USA Corp., CA) with a radius of 150 nm and a spring constant of 42 N/m was used. Under one normal load (2–6 μN), nanoscratch was performed in one dimension for 1.5 μm with slow scan disabled, back and forth repetitively for 10 times, at a sliding speed of 374.64 nm/s. The justification for selecting the range of load is detailed in the Results and Discussion. One tip was used for one set of nanoscratch tests, which included triplicate scratches under one load for five loads in total, consecutively. Following the nanoscratch experiment, we switched to a sharp tip (AC240TS-R3, radius of 7 nm, 70 Hz, 2 N/m, Oxford Instruments Company) to image the scratched area in AC/tapping mode (4 × 4 μm² for 512 lines and 512 points/line). The topography images were analyzed using Gwyddion to calculate the volume of the scratched area (details in the SI). For each sample, one set of nanoscratch tests was repeated on 3–5 different pieces of coupons (*n* = 8–13 under each load).

Nanoindentation Experiments. Elastic modulus and hardness of LDPE films were obtained by nanoindentation experiments using AFM.^{61–63} Compared to the widely used tensile tests that interrogate bulk properties,^{64–66} nano-indentation can provide surface nanomechanical properties, which are more relevant to the nanoscale surface wear. A spherical SiO probe (CP-FM-SiO-A, NANOSENSORS, Switzerland) with a spring constant of 2.8 N/m and a radius of 1000 nm was used (Figure S3). For each LDPE sample, 30 force curves were collected on random locations of 2 different

coupons. The force curves were fitted to the appropriate contact mechanics model based on the transition parameter using a customized MatLab code to calculate the elastic modulus and hardness of LDPE samples (SI).

Surface Chemistry, Molecular, Structural, and Morphological Characterization of LDPE. The experimental details of characterization and analysis of the carbonyl index ($CI = \frac{I_{1715}}{I_{1472}}$),⁶⁷ contact angle, molecular weight, surface roughness, bulk crystallinity, and photothermal AFM-IR of the pristine and UV-aged LDPE are included in SI using well-established methods.

RESULTS AND DISCUSSION

Photooxidation Leads to Oxidation, Chain Scission, and Chemicrystallization. A combination of characterization techniques evidenced substantial chain scission, oxidation, and chemicrystallization because of the photo-oxidation of LDPE (Figure 1). ATR-FTIR (Figures 1A and

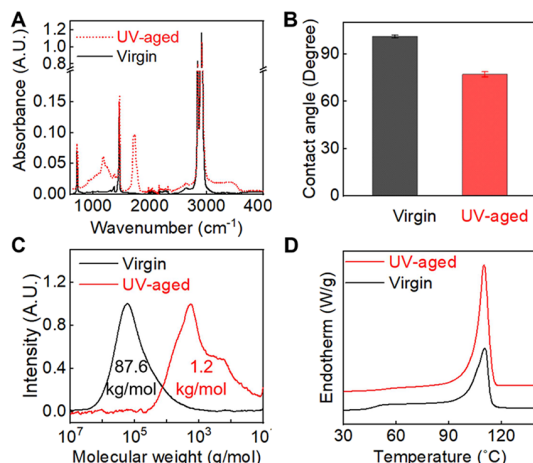


Figure 1. Photowathering under UVA at 60 °C led to oxidation, chain scission, and chemicrystallization of LDPE. (A) IR spectra showed a 63-fold increase in the carbonyl index (1713 cm^{-1}). (B) Decreased contact angle suggested an increase in hydrophilicity. (C) GPC traces showed a near 100-fold reduction in weight-average MW. (D) DSC thermogram showed a 2-fold increase in χ_c (23–43%). LDPE with a thickness of 101.6 μm was UV-aged in air for 50 days using a modified ASTM G154 method without condensation (1.55 W/m^2 , 340 nm, 60 °C).

S4A,B) results suggested a substantial increase in carbonyl groups ($1650\text{--}1850\text{ cm}^{-1}$) for LDPE after photooxidation, with the carbonyl index (CI) increased from 0.011 to 0.694 (peak area increased from 0.19 to 8.2 in $1650\text{--}1850\text{ cm}^{-1}$), consistent with many previous observations.^{68–70} The carbonyl group can be deconvolved into ketones or carboxylic acids ($1710\text{--}1713\text{ cm}^{-1}$) and esters and/or aldehydes (1734 cm^{-1}) as products of photooxidation. Furthermore, AFM-IR imaging analysis showed that the carbonyl peak intensity (1713 cm^{-1}) was minimal across the thickness of the virgin LDPE (Figures S5 and S6); in comparison, a clear carbonyl peak appeared homogeneously over the entire 100 μm thickness of the UV-aged LDPE. These results further demonstrate that our UV-aged LDPE was homogeneously oxidized across the thickness and completely embrittled. The IR-detected oxidation was consistent with increased hydrophilicity measured as a decline from 101.3 ± 0.8 to 77.2 ± 1.6 in the contact angle of LDPE

after photooxidation (Figure 1B). A similar reduction in contact angle after UV exposure was observed.^{24,71–73} In addition, chain scission was observed up to nearly two orders after photooxidation according to high-temperature GPC (from 87.6 to 1.2 kg/mol) (Figure 1C). Finally, we observed a 2-fold increase in the degree of crystallinity (23.3 ± 0.3 to $43.1 \pm 1.4\%$) after photooxidation by DSC analysis (Figures 1D and S4C), measured as the enthalpy of fusion at the melting temperature of the sample relative to that of a perfect crystal (293.6 J/g⁷⁴). Such an increase in crystallinity due to photooxidation has been referred to as chemicrystallization,⁷⁴ in which the broken chains have sufficient mobility to recrystallize along the existing lamellar structures. In addition, we observed facile breakage of the film, while it was being transferred using a tweezer. This is qualitative evidence that the ductile LDPE has been embrittled so that the strain at break is likely near zero.

Photooxidation Increases Wearless Sliding Friction and Delays the Onset of Wear of LDPE. *Wearless Sliding Friction.* Wearless frictional contact is the first solid–solid interaction prior to wear, which also contributes to abrasive wear. The wearless frictional regime is the linear regime of friction force (f) versus the normal load (F). For virgin LDPE, we observed such linearity ($R^2 > 0.98$) with normal load up to 335.16 ± 103.32 nN ($n = 5$, Figures 2A, S7 and Table S2) and $f < 17$ nN. The kinetic friction coefficient, $\mu = \frac{f}{F}$, was calculated to be 0.031 ± 0.004 ($n = 5$). Similar friction coefficients were found for PE (0.06)⁷⁵ and HDPE (0.1)⁷⁶ using comparable tip size and normal load. In comparison, photooxidized LDPE had a μ value of 0.066 ± 0.002 (Figures 2A, S8 and Table S2), 2-fold higher than that of virgin LDPE (paired t test, $p \leq 0.05$) and an overall higher f (< 50 nN). Spatial mapping of wearless f (Figure 2B–D revealed that the average f of LDPE was 1.72-fold higher after photowathering (42.78 ± 10.18 nN compared to 24.77 ± 4.89 nN, $p = 0 < 0.05$). Furthermore, the higher variance of f suggested a more heterogeneous surface in terms of friction after photowathering. We note that spatial friction force was not associated with topographical details (Figure S9).

The friction of polymers can result from (1) internal viscoelastic dissipation⁷⁷ from tip-polymer interaction affected by crystallinity⁷⁸ and glass transition temperature (T_g),⁷⁹ (2) noncovalent surface chemical interactions,⁸⁰ and (3) surface roughness relative to the size of the counterpart.^{81,82} First, a more crystalline LDPE would have reduced energy dissipation and friction force,⁸³ opposite to what we observed. Similarly, a previous outdoor weathering study on HDPE revealed an increase in T_g and a decrease in free volume,⁸⁴ which would have also led to lower friction. Second, the enhanced polarity and hydrophilicity of the oxidized LDPE surface (Figure 1A, B) will induce a stronger dipole–dipole interaction between the tip and sample, leading to higher friction force.⁷² Third, surface roughness of UV-aged LDPE was higher (Figure 2E): R_{RMS} increased from 4.31 ± 0.33 to 9.44 ± 1.12 nm (Figures 2F, G and S10), consistent with previous findings.^{66,73} Furthermore, the lateral feature analyzed by the power spectral density function (PSDF) (Figure 2H) and topography images (Figures S11 and S12) suggested that a significant fraction of the lateral features of both samples was lower than the size of the AFM tip (Figure 2E). Therefore, the measured friction resulted from multi-asperity contacts between the tip and samples. From the PSDF plots, the amplitude at all

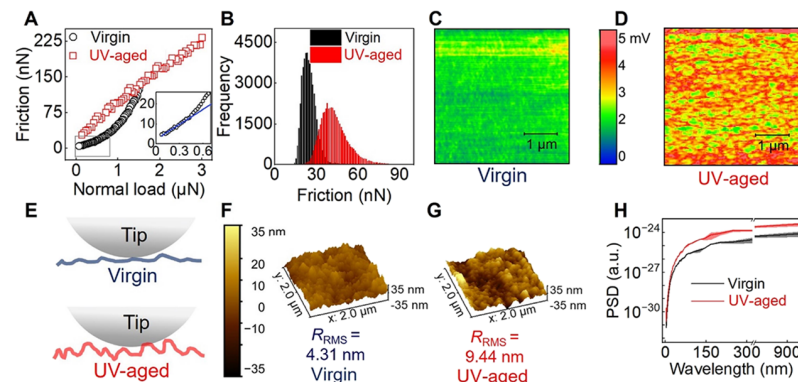


Figure 2. (A) Friction vs normal load curve for virgin and photooxidized LDPE. Inset: A representative of friction-to-wear transition (onset of wear) for virgin LDPE. (B) Histograms of friction under 50 nN load over a $4 \times 4 \mu\text{m}$ area, $n = 3 \times 49,152$ data points for 3 different locations on each sample. The friction of virgin LDPE ranged from 0.11 to 57.02 nN with a variance of 23.87 nN, in comparison to 5.38–113.45 nN for UV-aged LDPE (variance of 103.54 nN). A representative friction image of (C) virgin LDPE, and (D) UV-aged LDPE (data shown in B). (E) Illustration of the multi-asperity contact between tip and LDPE surface, where UV-aged LDPE had a higher roughness at all lateral scales. Topography images of (F) virgin LDPE and (G) UV-aged LDPE and the calculated root-mean-square roughness (R_{rms}). (H) Linear power spectral density function plotted with wavelength (inverse of spatial frequencies multiplied by 2π) demonstrated a higher frequency of lateral roughness features for UV-aged LDPE compared to virgin LDPE.

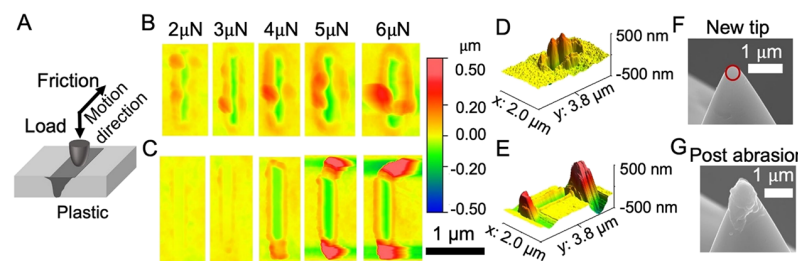


Figure 3. (A) Illustration of the single asperity nanoscratch test using LFM. Nanoscale wear topography with increasing load for (B) virgin and (C) UV-aged LDPE suggested a clear wear mechanism transition from plowing/wedge formation to cutting wear due to photowathering and load. The three-dimensional (3D) image of the abraded area of (D) virgin and (E) UV-aged LDPE under 4 μ N. The pile-up refers to the orange to red area accumulated around the scratch, and the scratch refers to the yellow to green color inside the groove or the scratch itself. We note that the presented scratch topography was obtained after 10 repeated sliding events. SEM image of 150 nm radius rounded silicon tip (F) before and (G) post nanoscratch experiment, suggesting transfer of polymer to tip. The post-abrasion SEM image of the tip was taken after being used for creating 15 scratches (i.e., 3 repeated scratches under each load from 2 to 6 μ N).

wavelengths was higher for the UV-aged LDPE, further suggesting that UV exposure increased the roughness of the entire size range of the lateral features. Our detailed analyses revealed that a higher nanoscale wearless sliding friction of LDPE after photowathering was mainly derived from surface chemistry/energy and roughness-dependent multi-asperity interactions.

Onset of Wear. When increasing the load to near the wear point (onset of wear), the lateral signal will have an additional contribution from material deformation (wear), leading to a distinct change in the slope of a friction force versus load curve⁴⁷ (Figure 2A, inset). Measuring the onset of wear could inform the critical load and energy input to trigger NPs generation from the nanoscale abrasive wear of LDPE. For virgin LDPE, the wear point was around 335.16 ± 103.32 nN ($n = 5$, Figure S5 and Table S2). Surprisingly, we observed no clear change of the slope for UV-aged LDPE up to 3 μ N load ($n = 5$, Figure S6 and Table S2), suggesting an over 1 order of magnitude suppression of the onset of wear, derived from photowathering. The result indicates that it requires more input of force and energy to initiate NPs release via the nanoscale abrasive wear mechanism for UV-aged LDPE. This is counterintuitive to the prevailing understanding that

photooxidized PE, PP, PS, PET, thermoplastic polyurethane, and polyamide are more likely to release MP/NPs.^{28,85,69,86} Details of the underlying mechanisms are discussed next. The gravitational force of one single sand grain with typical diameters that can undergo creep motion^{87,88} in the air can provide 2 nN to 13 μ N force (SI). Therefore, our finding on the onset of wear suggests that there could be a critical sand grain size that leads to the onset of abrasion of LDPE, which is UV-aging-dependent. We note that photowathering alone can directly lead to NP release in aqueous environments, through other release mechanisms (in the presence of water^{16,86} surfactants,¹⁹ and fluid shear stress). This is the first report that UV-aged LDPE can delay the onset of wear at the nanoscale.

Novel Nanoscratch Test Reveals Transition of Nano-scale Wear Mechanism during Photowathering. Our AFM-based nanoscale abrasive wear tests using μ N range forces and a 300 nm diameter silicon tip were performed on LDPE to simulate abrasion by rolling and sliding sand (Figure 3A). This range of load can represent the estimated gravitational force of one single sand grain described above^{87,88} (SI). More importantly, our nanoscratch tests can detail the wear mechanism at the single asperity level, which was not possible with other degradation and wear methods.

For virgin LDPE, abrasive wear under $F = 2\text{--}6 \mu\text{N}$ created scratch topographies (i.e., grooves) with a depth ranging from 50 to 300 nm and a width ranging from 100 to 500 nm (Figures S13 and S14). The abraded materials were pushed outside of the scratch and piled up around the periphery of the scratch (Figure 3B,D). These pile-up materials had nanometer to sub- μm features, with a height of $\sim 50\text{--}300 \text{ nm}$ and a width of $\sim 100\text{--}500 \text{ nm}$, which can be NPs if released. These features were typically long and thin, with some areas being “wavy” and partially covering the apparent scratch area. In addition, polymer transfer onto tips was observed after nanoscratch experiments (Figure 3E, G), indicating co-occurring adhesive wear^{35,36,89} (deformation by sliding of two surfaces with similar hardness). Such adhered polymer can be released as NPs via subsequent sand collision, or co-transport with sand.

In comparison, UV-aged LDPE had a lower scratch depth from near zero to 150 nm and a similar width as virgin LDPE (Figure S14). At load $>4 \mu\text{N}$, distinctively, the abraded materials were pushed and accumulated at the scratch ends, with little material remaining along the side of the scratch (Figure 3C, E). The pile-up features at scratch ends were fragment and sphere-like (compared to ribbon or flake-like observed in virgin polymer⁷⁸ and steel⁹⁰) and had a width of up to $1 \mu\text{m}$ and a height of up to 500 nm. Releasing the entire pile-up at the scratch end would lead to the formation of a near- μm -range NPs particle.

Kato and co-workers^{90–92} defined three wear mechanisms for microscale abrasive wear of metals based on in situ scanning electron microscopy observation. Plowing refers to groove formation and deformed material accumulation along the scratch. Cutting refers to wear debris being pushed to the scratch end continuously during sliding. Wedge formation is between plowing and cutting, where only the initially formed wear debris during sliding can accumulate at the scratch end. Our scratch topography of virgin LDPE clearly suggested a plowing and wedge formation mechanism,⁹⁰ which was transitioned to primarily cutting wear for the UV-aged LDPE at $4\text{--}6 \mu\text{N}$. The observed differences in wear mechanism between virgin and UV-aged LDPE are likely related to the difference between the wear of a ductile and brittle material, generally observed for metals and polymer composites.^{91,93,94} Furthermore, at $2\text{--}3 \mu\text{N}$, the wear mechanism of UV-aged LDPE remained at plowing and wedge formation, suggesting that the wear mechanism changed as a function of load, more so for UV-aged LDPE than virgin ones (Figure 3C). This load-dependent wear mechanism transition was previously discovered by Kato⁹¹ for microscale wear of metals and steels (plowing \rightarrow wedge formation \rightarrow cutting). This is the first time that the wear mechanism transition of LDPE was revealed after UV exposure. Such distinct wear mechanisms can imply a change in the wear rate, in other words, NPs release rate (next section).

Other wear modes including fatigue wear and crack formation generating micrometer-to-millimeter-scale debris have been widely observed for polymer materials by micro- and macroscale wear studies.^{24,26,43,95} Notably, we did not observe such types of wear for virgin LDPE in our study. Surprisingly, cracking was not observed for the completely embrittled UV-aged LDPE. This might be due to the presence of additives (e.g., antioxidants), which require further investigation. Our results clearly suggested a distinct wear mechanism at the nanoscale (plowing/cutting) and in the

investigated force range compared to the findings from macroscale studies (fatigue/cracking).

First Estimation of the Nanoscale Abrasive Wear Rate of LDPE at the Single Asperity Level. NPs are released from abrasion when the deformed material is either transferred onto the abrasive particle (Figure 3F, G) or detached from the original surface. The three mechanisms of wear described above were originally categorized by Kato et al.^{90–92} based on their likelihood of loose-wear debris release. In cutting wear, pile-up materials are physically moved to the scratch end, strongly implying the complete detachment of the pile-up from the original surface. Specifically, Kayaba et al.⁹⁰ observed that the cutting wear debris volume could grow as sliding continued. In comparison, the scratch end pile-up material in wedge formation did not change along with continuous sliding, suggesting that only initially deformed material can be released as debris. Plowing wear led to little direct debris release but the ridges could be removed by subsequent sliding.²⁶ Indeed, our results reveal that NP release by sand abrasion is a two-step process, including plastic deformation and wear debris release. By quantitatively analyzing the topography of the abraded area, we could first reveal the volume of deformed material, and their wear mechanism could inform the likelihood of the deformed material release as NPs.

Image analysis of the topography of the abraded area can calculate volumes of pile-up or scratch features (Figure 4A, B). Both scratch and pile-up volumes increased linearly with the load ($R^2 > 0.94$), following the Archard law;⁹⁶ notably, the pile-up volume was 2.8–4.6 and 3.7–8.4 times higher than the scratch volume, for virgin and UV-aged LDPE, respectively (Figure 4C, D). The higher pile-up over scratch volume is likely due to (1) pile-up material partially covering the scratch

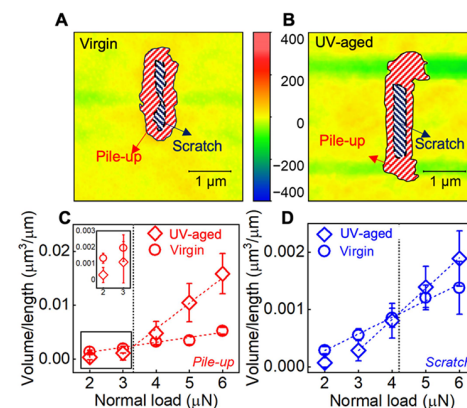


Figure 4. Nanoscale abrasive wear volume per sliding distance of UV-aged and virgin LDPE as an approximate of nanoplastic generation at the single asperity level. Representative topography images of (A) virgin and (B) UV-aged LDPE illustrate the raw topography data used for calculating pile-up and scratch volumes. The pile-up volume refers to the red strip highlighted area, and the scratch volume refers to the blue strip highlighted area. The pile-up volume was always higher than the scratch volume for both LDPE samples. (C) Pile-up and (D) scratch volume per length of UV-aged LDPE are higher than that of virgin LDPE (note the difference in the scale of the two figures). However, the wear rate of LDPE was reduced after photowathering at $2\text{--}3 \mu\text{N}$ (inset). Photowathering does *not* always increase the wear rate of LDPE. The vertical dashed line indicates the load where the UV-aged LDPE started to have a higher wear than virgin LDPE. For each sample, there were 8–13 repeated wear volume data under each load.

area, leading to a lower measured scratch volume than the actual volume (Figure S13), and (2) the elastic relaxation of the scratch due to the viscoelasticity of LDPE.⁹⁷ This is further supported by the smaller scratch height profiles than the tip geometry (Figure S14). Previous microscale wear of PE by sand grain impacts revealed that the relaxation can occur within a few hours of the impact and the scratch volume can be reduced up to 90% during 4 weeks.⁹⁸ Nevertheless, this result implies that pile-up volume is a more reliable and relevant measure of NPs generation compared to scratch volume; thus, our following analysis focused on the pile-up volume.

Using pile-up volume data, the nanoscale abrasive wear coefficient of virgin LDPE, expressed in units of $\mu\text{m}^3/\mu\text{N}$ sliding distance/ μN normal load (slope of Figure 4C), was measured and calculated to be 1.0×10^{-3} at the single asperity level. Only data from 3 to 6 μN were used for calculating this slope because of the near-zero wear rate at 2 μN for UV-aged LDPE (discussed in the next section). This wear rate is lower than previously reported wear rates for PEs performed under macroscale wear (Figure S15), likely due to the difference in asperity size and load-dependent wear mechanism.⁹⁹ In comparison, the wear coefficient of the UV-aged LDPE was 4.9 times higher ($4.9 \times 10^{-3} \mu\text{m}^3/\mu\text{m}/\mu\text{N}$). Furthermore, the lateral signal and its slope with the load during the nanoscratch test was around 3-fold lower for UV-aged LDPE (Figure S16), implying that it required less energy transfer from frictional force to create abrasive wear for UV-aged LDPE compared to virgin ones. Furthermore, the potential NP release rate for UV-aged LDPE by the cutting mechanism is likely over 4.9 times higher than the rate for virgin LDPE by the plowing mechanism (see last section). Our finding suggests that virgin ductile LDPE tends to plastically deform rather than release NPs via cutting wear. This implies that the current laboratory-scale MP/NPs preparation methods using mechanical milling of virgin plastics^{100,101} may create particle properties distinct from environmental MP/NPs.

The impact of photooxidation on the overall abrasive wear rate of LDPE observed here was consistent with previous findings on MP release^{28,102} and the understanding of the impact of polymer properties on wear rates. From the mechanics of materials perspective, the widely used Ratner-Lancaster correlation¹⁰³ predicts that the wear rate correlates with the reciprocal product of ultimate stress and the strain at break. The completely embrittled LDPE in this study had near-zero stress and strain at break, supporting the higher wear coefficient. In the space of molecular and structural properties of semicrystalline polymers, some recent studies highlighted the important role of interlamellar phase properties including chain entanglement,⁹⁹ tie chain,^{104,105} and interphase fraction,¹⁰⁶ in reducing the propensity to wear. The entanglement of LDPE in this study was likely destroyed after two decades of MW reduction (Figure 1C), down to near entanglement molar mass for PE.¹⁰⁷ In addition, previous studies have evidenced interlamellar shrinking and the reduction of the tie chain in photooxidized PE.⁶⁵ Both evidence can support the increased wear rate of UV-aged LDPE.

Impact of Photooxidation on the Wear Rate of LDPE Is Load-Dependent. Despite the overall trend of increasing wear rate due to photowear, unexpectedly, at 2–3 μN , UV-aged LDPE had less visibly shallower scratches and less pile-up volume compared to virgin ones (Figure 3C). This can be further seen in the quantified wear rate (inset of Figure 4C,D). This resistance to wear is consistent with the observed

higher load at the onset of wear for UV-aged LDPE observed during friction measurements (Figure 2A). Clearly, in this load regime, the wear rate and polymer properties correlation for UV-aged LDPE disobey the previous findings detailed above. We hypothesize that this is likely attributed to an increase in crystallinity (Figure 1D) as well as nanoindentation hardness and elastic modulus (Figure 5). Nanoindentation results

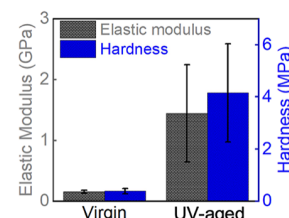


Figure 5. Increased hardness and elastic modulus of LDPE after photowathering. Photowathering caused the elastic modulus (left y-axis) to increase from 0.174 ± 0.027 GPa (virgin) to 1.627 ± 0.906 GPa (UV-aged). A similar trend was found for hardness (right y-axis), which was almost 11-fold higher for the UV-aged LDPE (4.67 ± 2.133 MPa) compared to the virgin LDPE (0.434 ± 0.113 MPa). The values were calculated by fitting the load and indentation depth using the JKR model, which was determined based on the adhesion-dependent transition parameter. Each force curve was collected with sufficient spacing (>3 times the probe diameter) between two indentation locations.

analyzed using a properly selected contact mechanics model (JKR model) suggested that photowathering increased the nanohardness and elastic modulus of LDPE by 10.7-fold and 9.3-fold, respectively. The increase in elastic modulus is consistent with previous tensile test results.⁶⁵ At the interfacial region, it takes a higher load (or pressure) to initiate plastic deformation of UV-aged LDPE which is opposed to the hardness. In addition, the tangential motion of sliding is opposed by wearless frictional force, which was also higher for UV-aged LDPE (Figure 2A). Both can be reflected as the coefficient of friction μ in the numerator and the hardness in the denominator of the RL correlation.¹⁰³ At a higher load (>4 μN), the abrasive wear rate is correlated with stress and strain at break which was substantially declined for UV-aged LDPE. To the best of our knowledge, this is the first time such unexpected wear behavior was revealed for UV-aged LDPE at the nanoscale, suggesting that NPs release does not always increase for LDPE after photowathering.

New Parameter to Evaluate the Wear Mechanism for LDPE Implying NP Release. Considering the complete process of NP release from nanoscale abrasive wear, the piled-up materials have to be released into free particles. While our method cannot directly observe this process, we hypothesize that the scratch-end pile-up materials in the cutting wear case are highly likely loose enough to be released easily. Indeed, a previously developed concept by Kato and co-workers^{90–92} developed a parameter named Degree of Wear to evaluate the propensity of releasing debris of given wear mechanisms. We adopted the concept to approximate the likelihood of pile-up material release as NPs. The Degree of Wear is defined as $\beta = \frac{A' - A''}{A'}$, where A' and A'' are the cross-sectional areas of the scratch (groove) and pile-up (ridge) at both sides of the scratch, respectively. As the scratch length is fixed, $A' - A''$ and A' correspond to the removable and total wear volume. Plowing has a $\beta \sim 0$, wedge formation has a $0 < \beta < 1$, and

cutting wear has a $\beta \sim 1$. However, this formula cannot directly be used for our samples or viscoelastic materials in general because (1) the scratch profile underestimates the total wear volume due to elastic relaxation of the scratch and (2) the cross-sectional area along the scratch varied significantly along the sliding direction (Figures 3 and S17). We propose a new degree of wear $\beta' = \frac{V''}{V'}$ for viscoelastic materials, where V'' is the volume of pile-up at the *scratch end* (dotted area shown in Figure 6A, B) and V' is the *total* pile-up volume. Our proposal

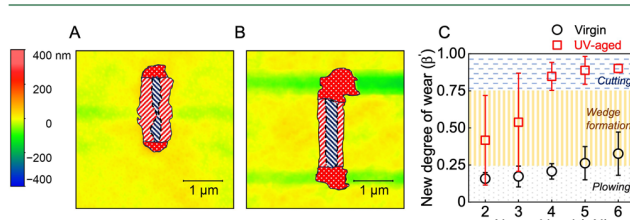


Figure 6. Proposed new Degree of Wear for elucidating the wear mechanism of viscoelastic materials. Representative topography images of (A) virgin and (B) UV-aged LDPE illustrate the raw topography data used for calculating pile-up volumes at the scratch end, where the red dotted area refers to the pile-up volume at the end. (C) β' quantitatively describes wear debris release via plowing, wedge formation, and cutting wear mechanisms. Note the large error bars of β' for 2 and 3 μN were due to that the <25 nm pile-up features were difficult to differentiate from the surrounding roughness.

of directly using measured wear volume can be better suited to calculate the ratio of the *removable wear volume* and the *total wear volume* that Kato and co-workers⁹⁰ intended to describe. For virgin LDPE, β' ranged from 0.15 to 0.32 from the entire 2–6 μN range. In comparison, the UV-aged LDPE had a β' of 0.41 and 0.53 for 2 and 3 μN normal loads, respectively, and β' ranged from 0.85 to 0.9 for 4–6 μN (Figure 6C). Based on our qualitative evaluation of the wear mechanism (Figure 4C, D), we propose regimes of β' to distinguish the wear mechanism: 0 $< \beta' < 0.25$: plowing wear, 0.25 $< \beta' < 0.75$: wedge formation, and 0.75 $< \beta' < 1$: cutting wear. The new β' can be used to describe the abrasive wear mechanism of other viscoelastic materials at the nanoscale. Our method of investigating nanoscale abrasives enabled this new and reliable way of evaluating the degree of wear for plastics. By multiplying the new β' with the wear rate estimated using pile-up volume, we report $0.4 \times 10^{-3} \mu\text{m}^3/\mu\text{m}/\mu\text{N}$ for virgin LDPE and $4.6 \times 10^{-3} \mu\text{m}^3/\mu\text{m}/\mu\text{N}$ for UV-aged LDPE. Considering this likelihood of release step, photodegradation may increase NP release by nanoscale abrasive wear by 10.6 times. We note that this is an initial estimation of NP release from the pile-up volume. We need future assessment of the characteristics of the pile-up materials, and the true NP release rate needs careful validation by further work.

■ ENVIRONMENTAL IMPLICATIONS

Our single asperity approach enabled by LFM elucidated new mechanistic insights into nanoscale abrasive wear that impacts NPs formation and potential release rates. This is a two-step process including (1) plastic deformation and (2) deformed material detachment into NPs. Our method enabled the exploration of nanoscale wear mechanisms (step 1) and can inform the second step of NP release. A lower rate of debris release for virgin LDPE is due to the plowing and wedge formation mechanism, compared to primarily cutting wear for

UV-aged LDPE implying high debris release. We also report that UV-aged LDPE is unexpectedly resistant to wear compared to virgin LDPE under gentle abrasion conditions. This suggests that it is harder for slow-moving fine sediments to abrade UV-aged LDPE than virgin LDPE. Furthermore, using our precise topography measurement, we proposed a modified Degree of Wear as an initial approximation for estimating the likelihood of NP release from the pile-up (second step). Finally, using a 300 nm size tip, we found that nanoscale abrasive wear exclusively generates NPs less than 1 μm .

A major contribution of our approach is the ability to calculate a wear rate with a unit of mass of NPs/load/time for the nanoscale abrasive wear process, compared to previously reported NPs/time with no characterization of mechanical stress,²⁸ or wear mass/load/distance.^{42,43} Such wear rate values will enable the conversion of laboratory-scale mechanical weathering study into actual plastic degradation under realistic environmental conditions without the need to test it under every single environmental scenario. Assuming the pile-up volume can be released as 100 nm NPs, we estimate potential NP release rates of 0.3 and 3.3 NPs/ $\mu\text{N}/\text{s}$ per sliding for virgin and UV-aged plastic, respectively, under the sliding velocity in this study. Considering velocities in creep aeolian transport (0–0.14 m/s), we expect up to 5×10^4 – 1×10^6 NPs/ $\mu\text{N}/\text{s}$ per sliding. NP release rate is 10 times higher after photodegradation of LDPE. This finding could be applied to other semicrystalline and rubbery polymer wastes (e.g., polypropylene),¹⁰⁸ and our tools can be applied to other plastic waste. Future work is needed to validate the probability or fraction that the pile-up volume can be released as NPs and how it can be impacted by abrasion conditions. Our initial estimation lays a critical foundation for determining true NP release via the nanoscale abrasive wear process.

Our findings on the nanoscale abrasive wear process can best simulate the creep transport of sand grains (i.e., rolling and sliding) with nanosize asperities on plastic films at the top layer of sand or soil column and can be applied to fluvial and swash zones in future studies. Recent field observations reported unique “rock-plastic complex”¹⁰⁹ and “plasticrust”¹¹⁰ in which plastic debris is integrated with inorganic rocks in river and shore environments, suggesting the environmental relevance and importance of sediment and plastic interactions. Creep is a major type of aeolian sand transport,^{87,88,111} fluvial,¹¹² and swash zone¹¹³ bedload movement. The NP release rate in aquatic sediment transport is likely higher due to a higher sediment transport velocity.¹¹⁴ Additional work is needed given the differences in creep sand size, friction, and wear between air and water. In addition, nanoscale abrasive wear of UV-aged plastic under aquatic conditions could also promote the release of dissolved organic carbon along with solid NPs. Ultimately, such rates can be converted into the specific surface degradation rate³⁴ to calculate the lifetime of plastics, enabling life cycle assessment of polymers that incorporate the end-of-life impacts.¹¹⁵

Finally, our findings reveal the difference in abrasive wear at the nanoscale compared to micro- and macroscales, which can lead to different implications regarding MP/NP release. In particular, the asperity size and load can impact the size of wear debris, rate, wear-polymer property correlations, and the role of photodegradation on wear. We highlight the need to study NP release by abrasive wear under *environmentally relevant* asperity size and applied load and to reveal the wear

mechanism if possible. Further studies are needed to expand our findings that were limited to the 300 nm asperity and a velocity ~ 4 orders of magnitude lower than the sediment velocities in air.⁸⁷

■ ASSOCIATED CONTENT

§ Supporting Information

The Supporting Information is available free of charge at <https://pubs.acs.org/doi/10.1021/acs.est.3c09649>.

Experimental details, AFM-IR results, replicates for the onset of wear and wear coefficient on LDPE samples, topographic images collected simultaneously with friction map, topographic images of LDPE samples, calculation of environmentally relevant forces, comparison of height profile among LDPE samples and the probe, horizontal view of 3D scratch, correlation of wear coefficient with crystallinity and molecular weight, lateral signal during nanoscratch experiment, and penetration depth under different normal loads ([PDF](#))

■ AUTHOR INFORMATION

Corresponding Author

Boya Xiong – Department of Civil, Environmental, and Geo-Engineering, University of Minnesota, Minneapolis, Minnesota 55455, United States;  orcid.org/0000-0002-7994-3508; Phone: +1 8149542509; Email: bxiong@umn.edu

Authors

Ehsanur Rahman – Department of Civil, Environmental, and Geo-Engineering, University of Minnesota, Minneapolis, Minnesota 55455, United States

Sara BinAhmed – Department of Civil, Environmental, and Geo-Engineering, University of Minnesota, Minneapolis, Minnesota 55455, United States

Phoebe Keyes – Department of Civil, Environmental, and Geo-Engineering, University of Minnesota, Minneapolis, Minnesota 55455, United States

Claire Alberg – Department of Civil, Environmental, and Geo-Engineering, University of Minnesota, Minneapolis, Minnesota 55455, United States

Stacy Godfrey-Igwe – Department of Mechanical Engineering, Massachusetts Institute of Technology, Cambridge, Massachusetts 02139, United States

Greg Haugstad – Characterization Facility, University of Minnesota, Minneapolis, Minnesota 55455, United States

Complete contact information is available at:

<https://pubs.acs.org/10.1021/acs.est.3c09649>

Author Contributions

[¶]E.R. and S.B. contributed equally to this work.

Notes

The authors declare no competing financial interest.

■ ACKNOWLEDGMENTS

This work was supported by the National Science Foundation Center for Sustainable Polymers headquartered at the University of Minnesota, Twin Cities, CHE-1901635. Parts of this work were carried out in the Characterization Facility, University of Minnesota, which receives partial support from the NSF through the MRSEC (Award Number DMR-2011401) and the NNCI (Award Number ECCS-2025124)

programs. The cover artwork was created in collaboration with John Beumer at the NSF Center for Sustainable Polymers.

■ REFERENCES

- (1) Thompson, R. C.; Olsen, Y.; Mitchell, R. P.; Davis, A.; Rowland, S. J.; John, A. W. G.; McGonigle, D.; Russell, A. E. Lost at Sea: Where Is All the Plastic? *Science* **2004**, *304* (5672), 838–838.
- (2) Rochman, C. M.; Browne, M. A.; Halpern, B. S.; Hentschel, B. T.; Hoh, E.; Karapanagioti, H. K.; Rios-Mendoza, L. M.; Takada, H.; Teh, S.; Thompson, R. C. Classify plastic waste as hazardous. *Nature* **2013**, *494* (7436), 169–171.
- (3) Bouwmeester, H.; Hollman, P. C. H.; Peters, R. J. B. Potential Health Impact of Environmentally Released Micro- and Nanoplastics in the Human Food Production Chain: Experiences from Nano-toxicology. *Environ. Sci. Technol.* **2015**, *49* (15), 8932–8947.
- (4) Shi, Q.; Tang, J.; Wang, L.; Liu, R.; Giesy, J. P. Combined cytotoxicity of polystyrene nanoplastics and phthalate esters on human lung epithelial A549 cells and its mechanism. *Ecotoxicology Environmental and Safety* **2021**, *213*, No. 112041.
- (5) Schwabl, P.; Köppel, S.; Königshofer, P.; Bucsics, T.; Trauner, M.; Reiberger, T.; Liebmann, B. Detection of Various Microplastics in Human Stool. *Annal of Internal Medicine* **2019**, *171*, 453–457.
- (6) Ji, Y.; Wang, C.; Wang, Y.; Fu, L.; Man, M.; Chen, L. Realistic polyethylene terephthalate nanoplastics and the size- and surface coating-dependent toxicological impacts on zebrafish embryos. *Environmental Science: Nano* **2020**, *7*, 2313–2324.
- (7) Kwak, J. I.; An, Y.-J. Microplastic digestion generates fragmented nanoplastics in soils and damages earthworm spermatogenesis and coelomocyte viability. *Journal of hazardous materials* **2021**, *402*, No. 124034.
- (8) Lian, J.; Wu, J.; Xiong, H.; Zeb, A.; Yang, T.; Su, X.; Su, L.; Liu, W. Impact of polystyrene nanoplastics (PSNPs) on seed germination and seedling growth of wheat (*Triticum aestivum* L.). *Journal of Hazardous Materials* **2020**, *385*, No. 121620.
- (9) Stubbins, A.; Law, K. L.; Muñoz, S. E.; Bianchi, T. S.; Zhu, L. Plastics in the Earth system. *Science* **2021**, *373* (6550), 51–55.
- (10) Revell, L. E.; Kuma, P.; Le Ru, E. C.; Somerville, W. R.; Gaw, S. Direct radiative effects of airborne microplastics. *Nature* **2021**, *598* (7881), 462–467.
- (11) Kvale, K.; Oschlies, A. Recovery from microplastic-induced marine deoxygenation may take centuries. *Nature Geoscience* **2023**, *16* (1), 10–12.
- (12) Ockelford, A.; Cundy, A.; Ebdon, J. E. Storm Response of Fluvial Sedimentary Microplastics. *Sci. Rep.* **2020**, *10* (1), 1865.
- (13) Gigault, J.; El Hadri, H.; Nguyen, B.; Grassl, B.; Rowenczyk, L.; Tufenkji, N.; Feng, S.; Wiesner, M. Nanoplastics are neither nanoplastics nor engineered nanoparticles. *Nat. Nanotechnol.* **2021**, *16* (5), 501–507.
- (14) Mitrano, D. M.; Wick, P.; Nowack, B. Placing nanoplastics in the context of global plastic pollution. *Nat. Nanotechnol.* **2021**, *16*, 491–500.
- (15) EFSA Panel on Contaminants in the Food Chain. Presence of nanoplastics and nanoplastics in food, with particular focus on seafood. *EFSA J.* **2016**, *14* (6), No. e04501.
- (16) Meides, N.; Menzel, T.; Poetzschner, B. R.; Löder, M. G.; Mansfeld, U.; Strohriegel, P.; Altstaedt, V.; Senker, J. R. Reconstructing the environmental degradation of polystyrene by accelerated weathering. *Environ. Sci. Technol.* **2021**, *55* (12), 7930–7938.
- (17) Hernandez, L. M.; Grant, J.; Fard, P. S.; Farmer, J. M.; Tufenkji, N. Analysis of ultraviolet and thermal degradations of four common nanoplastics and evidence of nanoparticle release. *Journal of Hazardous Materials Letters* **2023**, *4*, No. 100078.
- (18) Enfrin, M.; Lee, J.; Gibert, Y.; Basheer, F.; Kong, L.; Dumée, L. F. Release of hazardous nanoplastic contaminants due to nanoplastics fragmentation under shear stress forces. *Journal of hazardous materials* **2020**, *384*, No. 121393.
- (19) Pfohl, P.; Wagner, M.; Meyer, L.; Domercq, P.; Praetorius, A.; Hüffer, T.; Hofmann, T.; Wohlleben, W. Environmental degradation of nanoplastics: how to measure fragmentation rates to secondary

- micro-and nanoplastic fragments and dissociation into dissolved organics. *Environ. Sci. Technol.* **2022**, *56* (16), 11323–11334.
- (20) Yang, T.; Luo, J.; Nowack, B. Characterization of nanoplastics, fibrils, and microplastics released during washing and abrasion of polyester textiles. *Environ. Sci. Technol.* **2021**, *55* (23), 15873–15881.
- (21) Mattsson, K.; Björkroth, F.; Karlsson, T.; Hassellöv, M. Nanofragmentation of Expanded Polystyrene Under Simulated Environmental Weathering (Thermooxidative Degradation and Hydrodynamic Turbulence). *Frontiers in Marine Science* **2021**, *7*, No. 578178.
- (22) Hernandez, L. M.; Xu, E. G.; Larsson, H. C. E.; Tahara, R.; Maisuria, V. B.; Tufenkji, N. Plastic Teabags Release Billions of Microparticles and Nanoparticles into Tea. *Environ. Sci. Technol.* **2019**, *53*, 12300–12310.
- (23) Su, Y.; Hu, X.; Tang, H.; Lu, K.; Li, H.; Liu, S.; Xing, B.; Ji, R. Steam disinfection releases micro (nano) plastics from silicone-rubber baby teats as examined by optical photothermal infrared microspectroscopy. *Nat. Nanotechnol.* **2022**, *17* (1), 76–85.
- (24) Hadiuzzaman, M.; Salehi, M.; Fujiwara, T. Plastic litter fate and contaminant transport within the urban environment, photodegradation, fragmentation, and heavy metal uptake from storm runoff. *Environmental Research* **2022**, *212*, No. 113183.
- (25) Dawson, A. L.; Kawaguchi, S.; King, C. K.; Townsend, K. A.; King, R.; Huston, W. M.; Nash, S. M. B. Turning microplastics into nanoplastics through digestive fragmentation by Antarctic krill. *Nat. Commun.* **2018**, *9* (1), 1001.
- (26) Battacharjee, L.; Jazaei, F.; Salehi, M. Insights into the mechanism of plastics' fragmentation under abrasive mechanical forces: An implication for agricultural soil health. *Clean: Soil, Air, Water* **2023**, *51* (8), No. 2200395.
- (27) Ward, C. P.; Armstrong, C. J.; Walsh, A. N.; Jackson, J. H.; Reddy, C. M. Sunlight converts polystyrene to carbon dioxide and dissolved organic carbon. *Environmental Science & Technology Letters* **2019**, *6* (11), 669–674.
- (28) Song, Y. K.; Hong, S. H.; Jang, M.; Han, G. M.; Jung, S. W.; Shim, W. J. Combined effects of UV exposure duration and mechanical abrasion on microplastic fragmentation by polymer type. *Environ. Sci. Technol.* **2017**, *51* (8), 4368–4376.
- (29) Chubarenko, I.; Efimova, I.; Bagaeva, M.; Bagaev, A.; Isachenko, I. On mechanical fragmentation of single-use plastics in the sea swash zone with different types of bottom sediments: Insights from laboratory experiments. *Marine pollution bulletin* **2020**, *150*, No. 110726.
- (30) Bossa, N.; Sipe, J. M.; Berger, W.; Scott, K.; Kennedy, A.; Thomas, T.; Hendren, C. O.; Wiesner, M. R. Quantifying Mechanical Abrasion of MWCNT Nanocomposites used in 3D Printing: Influence of CNT content on abrasion products and rate of microplastic production. *Environ. Sci. Technol.* **2021**, *55* (15), 10332–10342.
- (31) Hebner, T. S.; Maurer-Jones, M. A. Characterizing microplastic size and morphology of photodegraded polymers placed in simulated moving water conditions. *Environmental Science: Processes & Impacts* **2020**, *22* (2), 398–407.
- (32) Cui, Q.; Yang, X.; Li, J.; Miao, Y.; Zhang, X. Microplastics Generation Behavior of Polypropylene Films with Different Crystalline Structures under UV Irradiation. *Polym. Degrad. Stab.* **2022**, *199*, No. 109916, DOI: 10.1016/j.polymdegradstab.2022.109916.
- (33) Ter Halle, A.; Ladirat, L.; Gendre, X.; Goudouneche, D.; Pusineri, C.; Routaboul, C.; Tenailleau, C.; Dupoyer, B.; Perez, E. Understanding the fragmentation pattern of marine plastic debris. *Environ. Sci. Technol.* **2016**, *50* (11), 5668–5675.
- (34) Chamas, A.; Moon, H.; Zheng, J.; Qiu, Y.; Tabassum, T.; Jang, J. H.; Abu-Omar, M.; Scott, S. L.; Suh, S. Degradation Rates of Plastics in the Environment. *ACS Sustainable Chem. Eng.* **2020**, *8* (9), 3494–3511.
- (35) Burwell, J. T., Jr Survey of possible wear mechanisms. *Wear* **1957**, *1* (2), 119–141.
- (36) Lancaster, J. K. Material-specific wear mechanisms: relevance to wear modelling. *Wear* **1990**, *141* (1), 159–183.
- (37) Lancaster, J. Abrasive wear of polymers. *Wear* **1969**, *14* (4), 223–239.
- (38) Sun, Z.; Mehmani, A.; Torres-Verdín, C. Subpore-Scale Trapping Mechanisms Following Imbibition: A Microfluidics Investigation of Surface Roughness Effects. *Water Resour. Res.* **2021**, *57* (2), No. e2020WR028324.
- (39) Bousbaa, C.; Madjoubi, M.; Hamidouche, Z.; Bouaouadja, N. Effect Of Sand Blasting On Soda Lime Glass Properties. *Eng. J. Univ. Qatar* **2003**, *16*, 125–138.
- (40) Ashby, M. F. Chapter 4 - Material Property Charts. In *Materials Selection in Mechanical Design* (Fourth ed.); Ashby, M. F., Ed.; Butterworth-Heinemann: 2011; pp 57–96.
- (41) Bullard, J. E.; Zhou, Z.; Davis, S.; Fowler, S. Breakdown and modification of microplastic beads by aeolian abrasion. *Environ. Sci. Technol.* **2023**, *57* (1), 76–84.
- (42) Yoon, E.-S.; Singh, R. A.; Oh, H.-J.; Kong, H. The effect of contact area on nano/micro-scale friction. *Wear* **2005**, *259* (7–12), 1424–1431.
- (43) Omar, M. K.; Atkins, A. G.; Lancaster, J. K. The role of crack resistance parameters in polymer wear. *J. Phys. D: Appl. Phys.* **1986**, *19* (2), 177.
- (44) Shipway, P.; Ngao, N. Microscale abrasive wear of polymeric materials. *Wear* **2003**, *255* (1–6), 742–750.
- (45) Bhushan, B. Nanotribology, Nanomechanics and Materials Characterization. In *Springer Handbook of Nanotechnology*; Bhushan, B., Ed.; Springer: Berlin Heidelberg, 2017; pp 869–934.
- (46) Tambe, N. S.; Bhushan, B. Nanoscale friction and wear maps. *Philos. Trans. R. Soc., A* **2008**, *366* (1869), 1405–1424.
- (47) Haugstad, G. *Atomic force microscopy: understanding basic modes and advanced applications*; John Wiley & Sons: 2012.
- (48) Celano, U.; Hsia, F.-C.; Vanhaeren, D.; Paredis, K.; Nordling, T. E.; Buijnsters, J. G.; Hantschel, T.; Vandervorst, W. Mesoscopic physical removal of material using sliding nano-diamond contacts. *Sci. Rep.* **2018**, *8* (1), 2994.
- (49) Walker, J.; Umer, J.; Mohammadpour, M.; Theodossiades, S.; Bewsher, S. R.; Offher, G.; Bansal, H.; Leighton, M.; Braunstingl, M.; Flesch, H.-G. Asperity level characterization of abrasive wear using atomic force microscopy. *Proc. R. Soc. A* **2021**, *477* (2250), No. 20210103.
- (50) Furustig, J.; Dobryden, I.; Almqvist, A.; Almqvist, N.; Larsson, R. The measurement of wear using AFM and wear interpretation using a contact mechanics coupled wear model. *Wear* **2016**, *350*–351, 74–81.
- (51) Tambe, N. S.; Bhushan, B. Nanoscale friction-induced phase transformation of diamond-like carbon. *Scripta Materialia* **2005**, *52* (8), 751–755.
- (52) Fang, T.-H.; Chang, W.-J.; Tsai, S.-L. Nanomechanical characterization of polymer using atomic force microscopy and nanoindentation. *Microelectronics Journal* **2005**, *36* (1), 55–59.
- (53) Fayolle, B.; Colin, X.; Audouin, L.; Verdu, J. Mechanism of degradation induced embrittlement in polyethylene. *Polym. Degrad. Stab.* **2007**, *92* (2), 231–238.
- (54) Liu, L.; Duan, H.; Zhan, W.; Zhan, S.; Jia, D.; Li, Y.; Li, C.; An, J.; Du, C.; Li, J. Effects of UV irradiation time on the molecular structure of typical engineering plastics and tribological properties under heavy load. *High Perform. Polym.* **2022**, *34* (3), 352–362.
- (55) Choudhury, M.; Hutchings, I. The effects of irradiation and ageing on the abrasive wear resistance of ultra high molecular weight polyethylene. *Wear* **1997**, *203*, 335–340.
- (56) Alshibli, K. A.; Alsaleh, M. I. Characterizing Surface Roughness and Shape of Sands Using Digital Microscopy. *J. Comput. Civil Eng.* **2004**, *18* (1), 36–45.
- (57) Rasmuson, A.; Pazmino, E.; Assemi, S.; Johnson, W. P. Contribution of nano-to microscale roughness to heterogeneity: Closing the gap between unfavorable and favorable colloid attachment conditions. *Environ. Sci. Technol.* **2017**, *51* (4), 2151–2160.

- (58) Altuhafi, F.; Coop, M. R.; Georgiannou, V. N. Effect of Particle Shape on the Mechanical Behavior of Natural Sands. *J. Geotech. Geoenviron. Eng.* **2016**, *142* (12), No. 04016071.
- (59) Yang, H.; Baudet, B. A.; Yao, T. Characterization of the surface roughness of sand particles using an advanced fractal approach. *Proceedings of the Royal Society A: Mathematical, Physical and Engineering Sciences* **2016**, *472* (2194), 20160524.
- (60) Hutter, J. L.; Bechhoefer, J. Calibration of atomic-force microscope tips. *Review of scientific instruments* **1993**, *64* (7), 1868–1873.
- (61) Tang, B.; Ngan, A.; Pethica, J. A method to quantitatively measure the elastic modulus of materials in nanometer scale using atomic force microscopy. *Nanotechnology* **2008**, *19* (49), No. 495713.
- (62) Briscoe, B.; Fiori, L.; Pelillo, E. Nano-indentation of polymeric surfaces. *J. Phys. D: Appl. Phys.* **1998**, *31* (19), 2395.
- (63) Dokukin, M. E.; Sokolov, I. On the measurements of rigidity modulus of soft materials in nanoindentation experiments at small depth. *Macromolecules* **2012**, *45* (10), 4277–4288.
- (64) Hsueh, H.-C.; Kim, J. H.; Orski, S.; Fairbrother, A.; Jacobs, D.; Perry, L.; Hunston, D.; White, C.; Sung, L. Micro and macroscopic mechanical behaviors of high-density polyethylene under UV irradiation and temperature. *Polym. Degrad. Stab.* **2020**, *174*, No. 109098.
- (65) Hsu, Y.-C.; Weir, M. P.; Truss, R. W.; Garvey, C. J.; Nicholson, T. M.; Halley, P. J. A fundamental study on photo-oxidative degradation of linear low density polyethylene films at embrittlement. *Polymer* **2012**, *53* (12), 2385–2393.
- (66) Ranjan, V. P.; Goel, S. Degradation of low-density polyethylene film exposed to UV radiation in four environments. *J. Hazard., Toxic, Radioact. Waste* **2019**, *23* (4), No. 04019015.
- (67) Syranidou, E.; Karkanorachaki, K.; Barouta, D.; Papadaki, E.; Moschovas, D.; Avgeropoulos, A.; Kalogerakis, N. Relationship between the Carbonyl Index (CI) and Fragmentation of Polyolefin Plastics during Aging. *Environ. Sci. Technol.* **2023**, *57* (21), 8130–8138.
- (68) Gulmine, J.; Janissek, P.; Heise, H.; Akcelrud, L. Degradation profile of polyethylene after artificial accelerated weathering. *Polym. Degrad. Stab.* **2003**, *79* (3), 385–397.
- (69) Mundhenke, T. F.; Li, S. C.; Maurer-Jones, M. A. Photo-degradation of polyolefin thin films in simulated freshwater conditions. *Environmental Science: Processes & Impacts* **2022**, *24* (12), 2284–2293.
- (70) Grause, G.; Chien, M.-F.; Inoue, C. Changes during the weathering of polyolefins. *Polym. Degrad. Stab.* **2020**, *181*, No. 109364.
- (71) Julienne, F.; Lagarde, F.; Delorme, N. Influence of the crystalline structure on the fragmentation of weathered polyolefines. *Polym. Degrad. Stab.* **2019**, *170*, No. 109012.
- (72) Garnai Hirsch, S.; Barel, B.; Segal, E. Characterization of surface phenomena: probing early stage degradation of low-density polyethylene films. *Polym. Eng. Sci.* **2019**, *59* (S1), E129–E137.
- (73) Suresh, B.; Maruthamuthu, S.; Kannan, M.; Chandramohan, A. Mechanical and surface properties of low-density polyethylene film modified by photo-oxidation. *Polym. J.* **2011**, *43* (4), 398–406.
- (74) Atkinson, C.; Richardson, M. Thermodynamic properties of ideally crystalline polyethylene. *Trans. Faraday Soc.* **1969**, *65*, 1764–1773.
- (75) Niederberger, S.; Gracias, D.; Komvopoulos, K.; Somorjai, G. Transitions from nanoscale to microscale dynamic friction mechanisms on polyethylene and silicon surfaces. *Journal of applied physics* **2000**, *87* (6), 3143–3150.
- (76) Cho, D.-H.; Bhushan, B. Nanofriction and nanowear of polypropylene, polyethylene terephthalate, and high-density polyethylene during sliding. *Wear* **2016**, *352*–353, 18–23.
- (77) Bahadur, S.; Ludema, K. C. The viscoelastic nature of the sliding friction of polyethylene, polypropylene and copolymers. *Wear* **1971**, *18* (2), 109–128.
- (78) Karuppiyah, K. K.; Bruck, A. L.; Sundararajan, S.; Wang, J.; Lin, Z.; Xu, Z.-H.; Li, X. Friction and wear behavior of ultra-high molecular weight polyethylene as a function of polymer crystallinity. *Acta Biomater.* **2008**, *4* (5), 1401–1410.
- (79) Hammerschmidt, J. A.; Gladfelter, W. L.; Haugstad, G. Probing polymer viscoelastic relaxations with temperature-controlled friction force microscopy. *Macromolecules* **1999**, *32* (10), 3360–3367.
- (80) Noy, A.; Frisbie, C. D.; Rozsnyai, L. F.; Wrighton, M. S.; Lieber, C. M. Chemical force microscopy: exploiting chemically-modified tips to quantify adhesion, friction, and functional group distributions in molecular assemblies. *J. Am. Chem. Soc.* **1995**, *117* (30), 7943–7951.
- (81) Fuller, K.; Tabor, D. The effect of surface roughness on the adhesion of elastic solids. *Proc. R. Soc. London, Ser. A* **1942**, *1975* (345), 327–342.
- (82) Archard, J. Elastic deformation and the laws of friction. *Proc. R. Soc. London, Ser. A* **1957**, *243* (1233), 190–205.
- (83) Haugstad, G.; Gladfelter, W. L.; Weberg, E. B.; Weberg, R. T.; Jones, R. R. Probing molecular relaxation on polymer surfaces with friction force microscopy. *Langmuir* **1995**, *11* (9), 3473–3482.
- (84) Xiong, J.; Ni, K.; Liao, X.; Zhu, J.; An, Z.; Yang, Q.; Huang, Y.; Li, G. Investigation of chemi-crystallization and free volume changes of high-density polyethylene weathered in a subtropical humid zone. *Polym. Int.* **2016**, *65* (12), 1474–1481.
- (85) Sørensen, L.; Groven, A. S.; Hovsbakken, I. A.; Del Puerto, O.; Krause, D. F.; Sarno, A.; Booth, A. M. UV degradation of natural and synthetic microfibers causes fragmentation and release of polymer degradation products and chemical additives. *Sci. Total Environ.* **2021**, *755*, No. 143170.
- (86) Liu, Z.; Zhu, Y.; Lv, S.; Shi, Y.; Dong, S.; Yan, D.; Zhu, X.; Peng, R.; Keller, A. A.; Huang, Y. Quantifying the Dynamics of Polystyrene Microplastics UV-Aging Process. *Environmental Science & Technology Letters* **2022**, *9* (1), 50–56.
- (87) Hong, C.; Xueyong, Z.; Chenchen, L.; Jiajia, H.; Yongqiu, W. Transport mass of creeping sand grains and their movement velocities. *Journal of Geophysical Research: Atmospheres* **2013**, *118* (12), 6374–6382.
- (88) Wang, Y.; Wang, D.; Wang, L.; Zhang, Y. Measurement of sand creep on a flat sand bed using a high-speed digital camera. *Sedimentology* **2009**, *56* (6), 1705–1712.
- (89) Aghababaei, R.; Warner, D. H.; Molinari, J.-F. Critical length scale controls adhesive wear mechanisms. *Nat. Commun.* **2016**, *7* (1), 11816.
- (90) Kayaba, T.; Hokkirigawa, K.; Kato, K. Analysis of the abrasive wear mechanism by successive observations of wear processes in a scanning electron microscope. *Wear* **1986**, *110* (3), 419–430.
- (91) Kato, K. Micro-mechanisms of wear—wear modes. *Wear* **1992**, *153* (1), 277–295.
- (92) Hokkirigawa, K.; Kato, K. An experimental and theoretical investigation of ploughing, cutting and wedge formation during abrasive wear. *Tribiol. Int.* **1988**, *21* (1), 51–57.
- (93) Soni, A.; Das, P. K.; Yusuf, M.; Ridha, S.; Kamyab, H.; Alam, M. A.; Masood, F.; Chelliapan, S.; Ubaidullah, M.; Pandit, B.; et al. Synergy of silica sand and waste plastics as thermoplastic composites on abrasive wear characteristics under conditions of different loads and sliding speeds. *Chemosphere* **2023**, *323*, No. 138233.
- (94) Alam, K. I.; Baratz, A.; Burris, D. Leveraging trace nanofillers to engineer ultra-low wear polymer surfaces. *Wear* **2021**, *482*, No. 203965.
- (95) Hutchings, I. M. Ductile-brittle transitions and wear maps for the erosion and abrasion of brittle materials. *J. Phys. D: Appl. Phys.* **1992**, *25* (1A), A212.
- (96) Archard, J. Contact and rubbing of flat surfaces. *Journal of applied physics* **1953**, *24* (8), 981–988.
- (97) Hadal, R. S.; Misra, R. D. K. Scratch deformation behavior of thermoplastic materials with significant differences in ductility. *Materials Science and Engineering: A* **2005**, *398* (1), 252–261.
- (98) Walley, S.; Field, J. E. The erosion and deformation of polyethylene by solid-particle impact. *Philos. Trans. R. Soc. London, Ser. A* **1987**, *321* (1558), 277–303.

- (99) Tervoort, T. A.; Visjager, J.; Smith, P. On abrasive wear of polyethylene. *Macromolecules* **2002**, *35* (22), 8467–8471.
- (100) McColley, C. J.; Nason, J. A.; Harper, B. J.; Harper, S. L. An assessment of methods used for the generation and characterization of cryomilled polystyrene micro- and nanoplastic particles. *Microplast. Nanoplast.* **2023**, *3* (1), 20.
- (101) Smith, C.; Brown, S.; Malone, N.; Bevers, S.; Renville, J.; Fairbrother, D. H. Nanoplastics prepared with uniformly distributed metal-tags: a novel approach to quantify size distribution and particle number concentration of polydisperse nanoplastics by single particle ICP-MS. *Environmental Science: Nano* **2024**, *11*, 911–923.
- (102) Sun, J.; Zheng, H.; Xiang, H.; Fan, J.; Jiang, H. The surface degradation and release of microplastics from plastic films studied by UV radiation and mechanical abrasion. *Science of The Total Environment* **2022**, *838*, No. 156369.
- (103) Lancaster, J. K. Relationships between the Wear of Polymers and their Mechanical Properties. *Proceedings of the Institution of Mechanical Engineers, Conference Proceedings* **1968**, *183* (16), 98–106.
- (104) Ferreira, E. H.; Fechine, G. J. High abrasive wear resistance polyethylene blends: an adapted Ratner–Lancaster correlation. *Polym. Bull.* **2022**, *79*, 3631–3648.
- (105) Klapperich, C.; Komvopoulos, K.; Pruitt, L. Tribological properties and microstructure evolution of ultra-high molecular weight polyethylene. *Journal of Tribology* **1999**, *121* (2), 394–402.
- (106) Zhang, H.; Zhao, S.; Xin, Z.; Ye, C.; Li, Z.; Xia, J. Wear Resistance Mechanism of Ultrahigh-Molecular-Weight Polyethylene Determined from Its Structure–Property Relationships. *Ind. Eng. Chem. Res.* **2019**, *58* (42), 19519–19530.
- (107) Raju, V. R.; Rachapudy, H.; Graessley, W. W. Properties of amorphous and crystallizable hydrocarbon polymers. IV. Melt rheology of linear and star-branched hydrogenated polybutadiene. *J. Polym. Sci., Polym. Phys. Ed.* **1979**, *17* (7), 1223–1235.
- (108) Fayolle, B.; Richaud, E.; Colin, X.; Verdu, J. degradation-induced embrittlement in semi-crystalline polymers having their amorphous phase in rubbery state. *J. Mater. Sci.* **2008**, *43* (22), 6999–7012.
- (109) Wang, L.; Bank, M. S.; Rinklebe, J.; Hou, D. Plastic–Rock Complexes as Hotspots for Microplastic Generation. *Environ. Sci. Technol.* **2023**, *57* (17), 7009–7017.
- (110) Gestoso, I.; Cacabelos, E.; Ramalhosa, P.; Canning-Clode, J. Plasticrusts: A new potential threat in the Anthropocene’s rocky shores. *Science of The Total Environment* **2019**, *687*, 413–415.
- (111) Nickling, W. The initiation of particle movement by wind. *Sedimentology* **1988**, *35* (3), 499–511.
- (112) Kramer, H. Sand mixtures and sand movement in fluvial model. *Transactions of the American Society of Civil Engineers* **1935**, *100* (1), 798–838.
- (113) Horn, D. P.; Mason, T. Swash zone sediment transport modes. *Marine Geology* **1994**, *120* (3), 309–325.
- (114) Hughes, M. G.; Masselink, G.; Brander, R. W. Flow velocity and sediment transport in the swash zone of a steep beach. *Marine Geology* **1997**, *138* (1–2), 91–103.
- (115) Maga, D.; Galatton, C.; Blömer, J.; Thonemann, N.; Özdamar, A.; Bertling, J. Methodology to address potential impacts of plastic emissions in life cycle assessment. *International Journal of Life Cycle Assessment* **2022**, *27* (3), 469–491.